Supplement of Biogeosciences, 18, 55–75, 2021
https://doi.org/10.5194/bg-18-55-2021-supplement

Biogeosciences Open Access EGU

Supplement of

Deepening roots can enhance carbonate weathering by amplifying CO_2-rich recharge

Hang Wen et al.

Correspondence to: Li Li (lili@engr.psu.edu)

The supplemental materials contain the detailed description of the study site Konza, and field and laboratory methods, the setup of reactive transport modeling, calculation of reactive transport times for Figure 6, derivation of equations for Ca and DIC concentrations, and carbonate chemistry data from fields for Figure 7.

S1. Description of the study site

Konza is a mesic native grassland where long-term (42 a, 2019) burning regime experiments across 60 watersheds has resulted in the encroachment of woody vegetation mostly in the riparian zone (Veach et al., 2014;Vero et al., 2018) (Figure S1). The average annual air temperature and precipitation is 13°C and ~835 mm, respectively (Nippert and Knapp, 2007;Hayden, 1998). The growing season is from April to September, when 75 % of the annual precipitation occurs. Konza also has frequent storms in almost any time of a year (Hayden, 1998). The bedrock of Konza contains repeating Permian couplets of 1-2 m thick limestone and slightly thicker mudstone (2-4 m) units (Macpherson, 1996). Limestone units are composed of primarily calcite with traces of dolomite (Macpherson et al., 2008), whereas mudstones are dominated by illite, chlorite, and mixed-layer clays of chlorite-illite and chlorite-vermiculite, varying in abundance from major to trace amounts (Macpherson and Sullivan, 2019). With an average thickness of 1-2 m in the lowlands, soils mostly have carbonate minerals less than 25 % with moderately low cation exchange capacities (Ransom et al., 1998). The soil is relatively thick and the water table is shallow so the response of groundwater to recharge events is rapid (Tsypin and Macpherson, 2012).

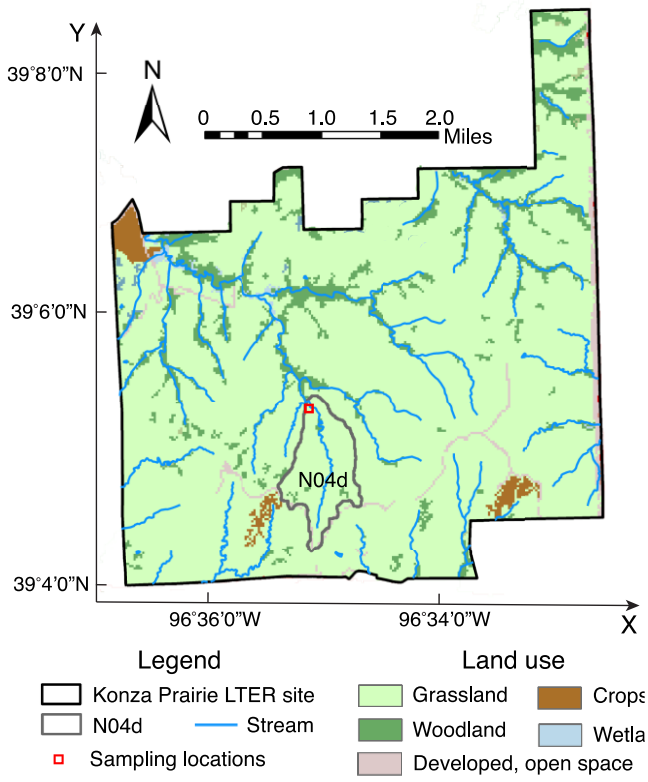

Figure S1. (A) Map of the Konza Prairie Long-Term Ecological Research site. Data here are from N04d.

Most of the Konza Prairie consists of grass species (e.g., big bluestem, *Andropogon gerardii*; little bluestem, *A. scoparius*; Indiangrass, *Sorghastrum nutans;* and switchgrass, *Panicum virgatura*) and native riparian gallery forest (oak, *Quercus spp.*; hackberry, *Celtis occidentalis*; and elm, *Ulmus Americana*) (Freeman, 1998). Watersheds with fire frequency return intervals of ~4 years or greater have incurred significant increase in woody vegetation on the hillslopes (e.g., dogwood, *Cornus drummondii*; sumac, *Rhus glabra*) and a pronounced increase in woody riparian vegetation (Veach et al., 2014) since the inception of the experimental design (Briggs et al., 2005).

S2. Field and laboratory methods

All field observation wells were made of 5-cm-diameter PVC pipe. Sampling occurred monthly during 2009-2010. Soil water was collected through soil-water samplers (Model 1900, Soil Moisture Equipment Co.) at three horizons, including 17, 153, and 366 cm. Soil gas wells were established at depths of 16, 84 and 152 cm so that the bottom hole of the gas well was at the same level as the midpoint of the water sampler's cup. 200 mL of soil gas was collected through a vacuum pump with Tygon® tubing into a 12 mL Exetainer® glass vial. More details are referred to Tsypin and Macpherson (2012).

Alkalinity of water samples was determined by titration with 0.02 N H_2SO_4. Concentrations of Cl were determined by suppressed ion chromatography (IC) with a Dionex 4000i (AG4A-SC and AS4A-SC columns and anion self-regenerating suppressor). Cations (Ca^{2+}, Mg^{2+}, Na^{+} and K^{+}) and dissolved Si ($H_4SiO_4(aq)$) were measured by inductively-coupled plasma-optical emission spectroscopy (JY 138 Ultrace ICP-OES) (detailed in Tsypin and Macpherson (2012)). Concentration of $CO_2(g)$ in the samples of soil gas was measured with an Agilent Technologies 6890N Gas Chromatograph.

S3. Model setup

Base case scenario with Konza field data. Soil mineralogy data indicated that as soil depth increases, anorthite ($CaAl_2Si_2O_8(s)$) and K-feldspar ($KAlSi_3O_8(s)$) decrease from 5.0 % (v/v soil phase) to 0 while calcite ($CaCO_3(s)$) increases from 0 to 10.0 % (v/v) (Wehmueller et al., 1993;Gunal and Ransom, 2005). Quartz and illite were relatively constant at around 40.0 % (v/v) (Table S1). For the base case model, the

shallow soils included anorthite, K-feldspar, and kaolinite in addition to calcite. Based on the average temperature measured at the top (soil surface) and bottom (groundwater) during the sampling period (Tsypin and Macpherson, 2012), soil temperature was assumed to decrease linearly with depth from 17 °C to 8 °C.

Table S1. Initial soil water chemistry, mineral compositions in different layers [a]

Chemical species	**Initial soil water chemistry**					**Ways obtained**
Aqueous species (mol/L except pH)	**Rainwater**	Horizon A (h = 17 cm)	Horizon AB (84 cm)	Horizon B (152 cm)	Groundwater (366 cm)	
pH[b]	6	6	6.2	6.8	7.0	Estimated[b]
Alkalinity	2.09×10^{-3}	2.09×10^{-3}	-	2.09×10^{-3}	2.09×10^{-3}	Measured
CO_2(aq)	1.23×10^{-5}	1.14×10^{-3}	1.74×10^{-3}	2.06×10^{-3}	8.54×10^{-4}	Estimated[c]
Cl	5.00×10^{-6}	1.74×10^{-3}	-	1.55×10^{-3}	6.06×10^{-4}	Measured
H_4SiO_4(aq)	1.00×10^{-4}	8.39×10^{-4}	-	7.89×10^{-4}	2.80×10^{-4}	Measured
Ca	2.06×10^{-5}	3.18×10^{-3}	-	3.75×10^{-3}	2.35×10^{-3}	Measured
Mg	1.00×10^{-6}	7.50×10^{-4}	-	9.04×10^{-4}	8.54×10^{-4}	Measured
Na	2.15×10^{-5}	3.39×10^{-3}	-	2.31×10^{-2}	4.35×10^{-4}	Measured
K	1.53×10^{-6}	3.97×10^{-4}	-	2.54×10^{-4}	2.09×10^{-4}	Measured
Gas						
CO_2(g) (%)		3.60	6.10	6.70	2.70	Measured
Mineral Volume Fraction (m^3/m^3)	h=0-54 cm	55-98 cm	99-145 cm	146-180 cm	181-366 cm	
Quartz	4.0×10^{-1}	4.0×10^{-1}	4.0×10^{-1}	4.0×10^{-1}	4.0×10^{-1}	Measured
Anorthite	5.0×10^{-2}	5.0×10^{-2}	5.0×10^{-2}	4.0×10^{-2}	0	Measured
Orthoclase	5.0×10^{-2}	5.0×10^{-2}	5.0×10^{-2}	4.0×10^{-2}	0	Measured
Calcite	0	5.0×10^{-3}	1.0×10^{-2}	1.5×10^{-2}	1.0×10^{-1}	Measured
Illite	4.0×10^{-1}	4.0×10^{-1}	4.0×10^{-1}	4.0×10^{-1}	4.0×10^{-1}	Measured
Kaolinite	1.0×10^{-1}	1.0×10^{-1}	1.0×10^{-1}	1.0×10^{-1}	1.0×10^{-1}	Measured

a. Initial species concentrations in soil water and CO_2(g) at measured horizon layers were from (Tsypin and Macpherson, 2012); The corresponding concentrations between measured horizon layers were interpolated linearly; Mineralogy composition were referred to (Macpherson, 1996;Macpherson et al., 2008).

b. The pH values in soil water were determined using measured alkalinity $C_A = C_{HCO_3^-} + 2C_{CO_3^{2-}} + C_{OH^-} - C_{H^+}$, $C_{HCO_3^-} = \frac{C_{CO_2(aq)}K_2}{C_{H^+}}$ and $C_{CO_3^{2-}} = \frac{C_{HCO_3^-}K_3}{C_{H^+}}$.

c. CO_2(aq) concentrations were estimated through Henry's law $C_{CO_2(aq)} = K_1 pCO_2$.

Rainfall chemistry is relatively constant across the year (Table S1). The initial conditions were estimated through a linear interpolation with depth based on the measurements at the three sampling locations (Figure 2A), including Horizon A (depth from the soil surface h =17 cm), Horizon AB (h =84 cm), Horizon B (h =152 cm), and Groundwater (h = 366 cm). The initial CO_2(aq) concentrations at the

sampling locations were estimated using Henry's law, i.e., $C_{CO_2,reference(aq)} = K_1 pCO_{2\,reference}$. The K_1 was temperature-dependent, following the van't Hoff equation:

$$K(T) = K_{25} exp\left(-\frac{\Delta H^{\circ}}{R} * \left(\frac{1}{T} - \frac{1}{273.15+25}\right)\right) \quad \text{(S1)}$$

Here K_{25} is the solubility in water at 293.15 K (25 °C); ΔH° is the standard enthalpy of the reaction and R is the gas constant (=8.314×10^{-3} kJ/K/mol); T is Kelvin temperature (K). For the dissolution of CO_2(g) (Reaction 1 in Table 1), $K_{1,25}$ (i.e., Henry's law constant) and ΔH_1° is 3.4×10^{-2} mol/kg/atm and -19.98 kJ/mol, respectively (Linstrom and Mallard, 2001).

In the model, $C_{CO_2(aq)}$ values were used as the "equilibrium constant" in the CrunchTope database for the combined reactions 0-1 (in Table 1) to become $CO_2(g^*) \leftrightarrow CO_2(aq)$. And as the parameter used to control the soil pCO$_2$ level in the model, the prescribed $C_{CO_2(aq)}$ value was both temporally- and spatially-dependent in the base case. The $C_{CO_2(aq)}$ values at different depths were interpolated linearly based on the estimation ($C_{CO_2(aq)} = K_1 p\mathrm{CO}_2$) at three sampling layers with monthly soil CO$_2$ data (Table 2). With an assumed linearly decreasing relationship with soil depth, soil temperature along depth was used as a track for CrunchTope and its database to obtain the $C_{CO_2(aq)}$ value for the corresponding soil depth. The $C_{CO_2(aq)}$ values along depth (associated linearly with soil temperature) were updated monthly through multiple CrunchTope database files (each month with one updated $C_{CO_2(aq)}$ database) through the CrunchTope "*restart"* and "save_restart" option. Thus, through the prescribed temporally (monthly) and spatially (depth) dependent $C_{CO_2(aq)}$, the soil pCO$_2$ concentrations were well simulated in the model compared to field data and further determined the dynamics of Ca and DIC, as have been shown in Section 4.1 and 5.1.

S4. Calculation of reactive transport times for Figure 6

In the term $kA_T\left[1 - exp\left(-\frac{\tau_{eq}}{\tau_a}\right)\right]$, $k_{calcite}$ is the intrinsic calcite kinetic rate constant measured under well-mixed conditions (10$^{-7.69}$ mol/m^2/s, Table 1) while A_T is total calcite surface area (m^3); τ_{eq} is the time for a mineral to reach equilibrium in a closed, well-mixed system: $\tau_{eq} = \frac{V_T \phi (C_{eq} - C_0)}{A_T k}$, where V_T is the

total domain volume (m^3); C_{eq} and C_0 are the equilibrium and initial Ca concentration (mol/m^3) respectively. For the cases with annual-average soil CO_2 in Scenario 1-3, C_{eq} was ~1.6 mol/m^3 (as shown in Figure 3) and τ_{eq} was estimated to be $10^{-4.34}$ years (0.40 hours). For the Konza base case, monthly soil CO_2 in September and March had the highest and lowest values respectively (Table 2), leading to corresponding equilibrium Ca concentrations and therefore different τ_{eq} values. The τ_{eq} in September and March was estimated to be $10^{-4.29}$ and $10^{-4.42}$ years respectively. In the heterogeneity factor $\left\{1 - exp\left[-L\left(\frac{\tau_a}{\tau_{ad,r}}\right)\right]\right\}^{\alpha}$, the shape factor α is determined by physical heterogeneity given by the permeability contrast between reactive and non-reactive zones. For the different flow partitioning cases, grassland (95 % vs. 5 %) vs. woodland (60 % vs. 40 %), we assumed α = 0.8 to represent a high heterogeneous field. The $\frac{\tau_a}{\tau_{ad,r}}$ quantifies the relative timescale of advection in the whole domain (residence time $\tau_a = \frac{L\phi}{Q_T}$) versus transport time in reactive zones ($\tau_{ad,r}$). The $\tau_{ad,r} = \frac{\tau_{a,r}\tau_{d,r}}{\tau_{a,r}+\tau_{d,r}}$ quantifies the transport time coupling diffusion/dispersion and advection in the calcite zones, where $\tau_{a,r}$ and $\tau_{d,r}$ are the average timescale of advection and diffusion/dispersion in the calcite zone, respectively. When $\frac{\tau_a}{\tau_{ad,r}} > 1$, reaction products transport out of the calcite zones faster than the domain residence time, leading to the negligible mass transport limitation caused by preferential flow paths and values of heterogeneity factor $\left\{1 - exp\left[-L\left(\frac{\tau_a}{\tau_{ad,r}}\right)\right]\right\}^{\alpha}$ approaching 1.0. In contrast, when $\frac{\tau_a}{\tau_{ad,r}}$ < 1, water mostly bypasses the reactive calcite zones, leading to significant influence of flow partitioning and the heterogeneity factor << 1.0. Calculated τ_a, $\tau_{a,r}$, $\tau_{d,r}$, and $\tau_{ad,r}$ and their corresponding weathering rates for Scenarios 1-3 are in Table S2. The calcite weathering rates (mol/a) are equivalent to the effluent Ca fluxes (shown in Figure 4).

Table S2. Calculated timescales in the grassland and woodland cases under different infiltration rates

Cases	*Infiltration rate (m/a)*	τ_a *(a)*	$\tau_{a,r}$ *(a)*	$\tau_{d,r}$ *(a)*	$\tau_{ad,r}$ *(a)*	$\frac{\tau_a}{\tau_{ad,r}}$	$R_{calcite}$ *(mol/a)*
$Grass_{PF}$	$10^{-1.4}$	4.7×10^{1}	8.0×10^{2}	4.7×10^{2}	2.9×10^{2}	1.6×10^{-1}	3.9×10^{-2}
$Wood_{PF}$			1.0×10^{2}	4.7×10^{2}	8.2×10^{1}	5.6×10^{-1}	4.6×10^{-2}
$Grass_{VF}$			4.0×10^{1}	4.7×10^{2}	4.0×10^{1}	1.3×10^{0}	5.9×10^{-2}

$Wood_{VF}$			4.0×10^{1}	4.7×10^{2}	4.0×10^{1}	1.3×10^{0}	6.0×10^{-2}
$Grass_{HF}$			0	4.7×10^{2}	4.7×10^{2}	1.0×10^{-1}	3.4×10^{-2}
$Wood_{HF}$			0	4.7×10^{2}	4.7×10^{2}	1.0×10^{-1}	3.3×10^{-2}
$Grass_{PF}$	$10^{-0.4}$	4.7×10^{0}	8.0×10^{1}	4.7×10^{2}	6.8×10^{1}	6.9×10^{-2}	1.8×10^{-1}
$Wood_{PF}$			1.0×10^{1}	4.6×10^{2}	9.8×10^{0}	4.8×10^{-1}	3.4×10^{-1}
$Grass_{VF}$			4.0×10^{0}	4.6×10^{2}	4.0×10^{0}	1.2×10^{0}	5.7×10^{-1}
$Wood_{VF}$			4.0×10^{0}	4.6×10^{2}	4.0×10^{0}	1.2×10^{0}	5.9×10^{-1}
$Grass_{HF}$			0	4.7×10^{2}	4.7×10^{2}	1.0×10^{-2}	1.2×10^{-1}
$Wood_{HF}$			0	4.7×10^{2}	4.7×10^{2}	1.0×10^{-2}	1.4×10^{-1}
$Grass_{PF}$	$10^{0.6}$	4.7×10^{-1}	8.0×10^{0}	4.6×10^{2}	7.8×10^{0}	6.9×10^{-2}	7.9×10^{-1}
$Wood_{PF}$			1.0×10^{-1}	4.4×10^{2}	1.0×10^{0}	4.7×10^{-1}	2.4×10^{0}
$Grass_{VF}$			4.0×10^{-1}	4.0×10^{2}	4.0×10^{-1}	1.2×10^{0}	5.3×10^{0}
$Wood_{VF}$			4.0×10^{-1}	4.0×10^{2}	4.0×10^{-1}	1.2×10^{0}	5.6×10^{0}
$Grass_{HF}$			0	4.7×10^{2}	4.7×10^{2}	1.0×10^{-3}	3.9×10^{-1}
$Wood_{HF}$			0	4.7×10^{2}	4.7×10^{2}	1.0×10^{-3}	3.4×10^{-1}

S5. Derivation of equations for thermodynamics of calcite dissolution and the dependence of equilibrium C_{Ca} and C_{DIC} on soil CO_2 and temperature

Combining Reactions 1 and 4 in Table 1, the overall reaction is $CaCO_3(s) + CO_{2(g)} + H_2O \leftrightarrow Ca^{2+} + 2HCO_3^-$, with its equilibrium constant can be expressed as:

$$K_t = \frac{a_{Ca^{2+}} a_{HCO_3^-}^2}{pCO_2} = K_1 K_4 \quad \text{(S2)}$$

The solutes follow the charge balance:

$$2C_{Ca^{2+}} + C_{H^+} = C_{HCO_3^-} + C_{OH^-} + 2C_{CO_3^{2-}} \quad \text{(S3)}$$

With the soil water pH typically lower than 8.3, $C_{CO_3^{2-}}$, C_{OH^-}, and C_{H^+} are negligible, such that the above equation can be simplified into

$$2C_{Ca^{2+}} = C_{HCO_3^-} \quad \text{(S4)}$$

Assuming relatively low salinity, activities are close to concentrations, the combination of Eq. S2 and S4 yield:

$$C_{Ca^{2+}} = \sqrt[3]{\frac{K_t \cdot pCO_2}{4}} \quad \text{(S5)}$$

$$C_{DIC} = C_{CO_2(aq)} + C_{HCO_3^-} + C_{CO_3^{2-}} \approx K_1 \cdot pCO_2 + 2\sqrt[3]{\frac{K_t \cdot pCO_2}{4}} \quad \text{(S6)}$$

Equilibrium constants are temperature-dependent and can be estimated using the van't Hoff equation (Eq. S1), the total equilibrium constant K_t ($= K_1 K_4$) can be estimated as:

$$K_t(T) = K_{t,25} exp\left(-\frac{\Delta H_t^\circ}{R} * \left(\frac{1}{T} - \frac{1}{298.15}\right)\right) \quad \text{(S7)}$$

Here $K_{t,25}$ (=$K_{1,25}K_{4,25}$, listed in Table 1) is $10^{-6.59}$ and $10^{-5.99}$ for "impure" and "pure" calcite, respectively; Note that the $K_{t,25}$ for "impure" calcite may vary by locations with differently mineralogy (Macpherson and Sullivan, 2019) and for this work was calibrated based on the data-model fit (Ca and alkalinity concentrations). The standard enthalpy ΔH_t° ($= \Delta H_1^\circ + \Delta H_4^\circ$, in Table 1) is -35.83 kJ/mol. The concentrations of Ca and DIC therefore can be estimated directly from temperature and pCO$_2$ following the equation:

$$C_{Ca} = \left[K_{t,25} \times e^{f(T)} \times p_{CO_2} \right]^{\frac{1}{3}} \quad \text{(S8)}$$

$$C_{DIC} = 2\left[K_{t,25} \times e^{f(T)} \times p_{CO_2} \right]^{\frac{1}{3}} + K_{1,25} \times e^{f(T)} \times p_{CO_2} \quad \text{(S9)}$$

Where $f(T) = -\frac{\Delta H_t^o}{4R}\left(\frac{1}{T} - \frac{1}{298.15}\right)$

Here $K_{t,25}$ is the equilibrium constant $K_t = \frac{a_{Ca^{2+}} a_{HCO_3^-}^2}{pCO_2} = K_1 K_4$ (Table 1) at 25°C; $K_{1,25}$ is the equilibrium constant of K_1 (Table 1) at 25°C; ΔH° is the standard enthalpy; R is the gas constant (=8.314×10^{-3} kJ/K/mol); T is Kelvin temperature (K). Eq. S8 and S9 suggest that Ca and DIC concentrations can be estimated directly from temperature, pCO$_2$, and thermodynamics (ΔH_t°).

S6. Carbonate chemistry data for Figure 7. These catchments meet the criteria of carbonate water chemistry: (Ca + Mg)/alkalinity molar ratio < 0.9, Ca/SO$_4$ >10, Ca/Na >12, Ca/Mg > 1, and charge balance

error < 10 % (Romero-Mujalli et al., 2019;Gaillardet et al., 1999). Overall, there are 162 data points, including pCO_2, Ca and DIC concentrations in spring water. The concentrations of CO_2(g), Ca and DIC in spring water were assumed to be similar to those in groundwater, which are often difficult and expensive to obtain.

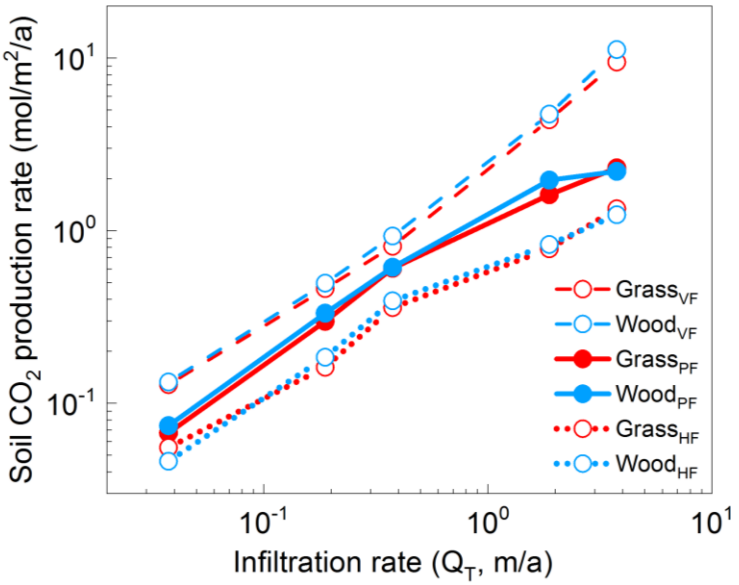

Figure S2. Soil CO_2 production rate as a function of infiltration rate under steady state in numerical experiments: $Grass_{PF}$ and $Wood_{PF}$ with flow partitioning, $Grass_{VF}$ and $Wood_{VF}$ with 100 % vertical flow (no flow partitioning), and $Grass_{HF}$ and $Wood_{HF}$ with 100 % lateral flow (no flow partitioning).

Reference

Briggs, J. M., Knapp, A. K., Blair, J. M., Heisler, J. L., Hoch, G. A., Lett, M. S., and McCarron, J. K.: An ecosystem in transition. Causes and consequences of the conversion of mesic grassland to shrubland, Bioscience, 55, 243-254, 10.1641/0006-3568(2005)055[0243:Aeitca]2.0.Co;2, 2005.

Freeman, C. C.: The flora of Konza Prairie: a historical review and contemporary patterns, Grassland dynamics: long-term ecological research in tallgrass prairie. Oxford University Press, New York, 69-80, 1998.

Gaillardet, J., Dupré, B., Louvat, P., and Allègre, C. J.: Global silicate weathering and CO2 consumption rates deduced from the chemistry of large rivers, Chem. Geol., 159, 3-30, 10.1016/S0009-2541(99)00031-5, 1999.

Gunal, H., and Ransom, M. D.: Clay mineralogy, specific surface area and micromorphology of polygenetic soils from Eastern Kansas, Archives of Agronomy and Soil Science, 51, 459-468, 2005.

Hayden, B. P.: Regional climate and the distribution of tallgrass prairie, Grassland dynamics: long-term ecological research in tallgrass prairie. Oxford University Press, New York, 19-34, 1998.

Linstrom, P. J., and Mallard, W. G.: NIST Chemistry webbook; NIST standard reference database No. 69, 2001.

Macpherson, G., and Sullivan, P. L. J. C. G.: Dust, impure calcite, and phytoliths: Modeled alternative sources of chemical weathering solutes in shallow groundwater, Chem Geol, 527, 118871, 10.1016/j.chemgeo.2018.08.007, 2019.
Macpherson, G. L.: Hydrogeology of thin limestones: The Konza Prairie Long-Term Ecological Research Site, Northeastern Kansas, J Hydrol, 186, 191-228, 10.1016/s0022-1694(96)03029-6, 1996.
Macpherson, G. L., Roberts, J. A., Blair, J. M., Townsend, M. A., Fowle, D. A., and Beisner, K. R.: Increasing shallow groundwater CO2 and limestone weathering, Konza Prairie, USA, Geochimica Et Cosmochimica Acta, 72, 5581-5599, 10.1016/j.gca.2008.09.004, 2008.
Nippert, J. B., and Knapp, A. K.: Soil water partitioning contributes to species coexistence in tallgrass prairie, Oikos, 116, 1017-1029, 10.1111/j.2007.0030-1299.15630.x, 2007.
Ransom, M. D., Rice, C. W., Todd, T. C., and Wehmueller, W. A.: Soils and soil biota: Grassland dynamics: long-term ecological research in tallgrass prairie. Long-term ecological research network series, Oxford University Press, New York 1998.
Romero-Mujalli, G., Hartmann, J., Börker, J., Gaillardet, J., and Calmels, D.: Ecosystem controlled soil-rock pCO2 and carbonate weathering–Constraints by temperature and soil water content, Chem Geol, 527, 118634, 10.1016/j.chemgeo.2018.01.030, 2019.
Tsypin, M., and Macpherson, G. L.: The effect of precipitation events on inorganic carbon in soil and shallow groundwater, Konza Prairie LTER Site, NE Kansas, USA, Applied Geochemistry, 27, 2356-2369, 10.1016/j.apgeochem.2012.07.008, 2012.
Veach, A. M., Dodds, W. K., and Skibbe, A.: Fire and Grazing Influences on Rates of Riparian Woody Plant Expansion along Grassland Streams, Plos One, 9, 10.1371/journal.pone.0106922, 2014.
Vero, S. E., Macpherson, G. L., Sullivan, P. L., Brookfield, A. E., Nippert, J. B., Kirk, M. F., Datta, S., and Kempton, P.: Developing a Conceptual Framework of Landscape and Hydrology on Tallgrass Prairie:A Critical Zone Approach, Vadose Zone Journal, 17, 10.2136/vzj2017.03.0069, 2018.
Wehmueller, W., Ransom, M., and Nettleton, W.: Micromorphology of polygenetic soils in a small watershed, north central Kansas, USA, in: Developments in Soil Science, Elsevier, 247-255, 1993.